Proceedings of ASME 2009 Seventh International Fuel Cell Science, Engineering and Technology Conference
FuelCell2009
June 8-10, 2009 Newport Beach, California, USA

FuelCell2009-85173

EXTRACTING MODEL PARAMETERS AND PARADIGMS FROM NEUTRON IMAGING OF DEAD-ENDED ANODE OPERATION

Jason B. Siegel *
Anna G. Stefanopoulou
Fuel Cell Control Laboratory
University of Michigan
Ann Arbor, Michigan, 48109

Serhat Yesilyurt
Faculty of Engineering & Natural Sciences
Sabanci University
Istanbul, Turkey

ABSTRACT

In a PEMFC, feeding dry hydrogen into a dead-ended anode (DEA), reduces the overall system cost, weight and volume due to reduced need for a hydrogen-grade humidification and recirculation subsystems, but requires purging to remove the accumulated water and inert gas. Although the DEA method of operation might be undesirable due to its associated high spatial variability it provides a unique perspective on the evolution of the water accumulation in the anode. Sections of the channel nearest the inlets are significantly drier than those nearest the outlet as shown in the neutron imaging of a 53 cm^2 PEMFC. This method allows in-situ visualization of distinct patterns, including water front propagation along the channels.

In this paper we utilize neutron imaging of the liquid water distributions and a previously developed PDE model of liquid water flow in the GDL to (a) identify a range of numerical values for the immobile saturation limit, (b) propose a gravity-driven liquid flow in the channels, and (c) derive the two-phase GDL boundary conditions associated with the presence of liquid water in the channel.

NOMENCLATURE

V_l GDL liquid water volume
V_p GDL open pore volume
W mass flux
N molar flux
p pressure
T temperature
$\mathcal{R}$ universal gas constant
A_{fc} fuel cell active area
s GDL liquid water saturation
s_{im} immobile saturation limit
ε GDL porosity
c concentration
D_v water vapor diffusivity
M_v water vapor molar mass
ρ_l liquid water density
ν_{mix} gas mixture kinematic viscosity
λ_{H_2} hydrogen excess ratio = (Utilization)$^{-1}$
i current density
t_w water thickness

INTRODUCTION

Feeding dry hydrogen to the anode of a Proton Exchange Membrane Fuel Cell (PEMFC) reduces the overall system cost, weight and volume due to reduced need for a hydrogen-grade humidification subsystem. However, when operating the anode with a dry hydrogen feed, it is commonly understood that the portion of the channel nearest the inlet will be significantly drier than the channel portion nearest the outlet. This condition may be problematic at higher current density, since the proton carrying capacity of the membrane depends on membrane hydration. A dry membrane is ineffective at transporting ions and hence pro-

*Address all correspondence to this author. Email: siegeljb@umich.edu

duces more heat, which further dries the membrane. Due to the slow gas flow velocity on the anode, and the low water vapor carrying capacity of the hydrogen gas stream, water removal from the anode is more difficult than the cathode. Numerous articles on liquid water droplet formation and removal from the surface of the Gas Diffusion Layer (GDL) have been published [1–4]. Neutron imaging work clearly illustrates the difficulty of liquid water removal [5]. A neutron image shown in Fig. 1, also clearly indicates the dry-inlet, wet-outlet phenomenon. Excessive amounts of water in the anode channel can cause a reversible degradation in cell voltage. This excess water can also lead to H_2 starvation and carbon corrosion if additional conditions, such as high potential, occur simultaneously [6, 7].

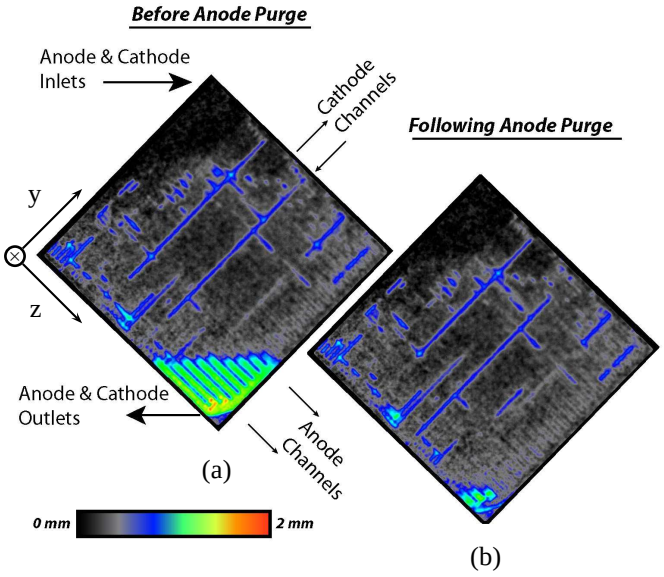

Figure 1. Neutron images of the fuel cell active area showing liquid water thickness in mm [5]. The cell was operated at 566 mA cm^{-2}, 55 °C, with fully humidified air at 50 % oxygen utilization for cathode and dry hydrogen supplied to anode. (a) excessive anode flooding observed after 15 minutes of 100% H_2 utilization. (b) some cathode channel flooding remained after 2 seconds of a 5% H_2 utilization

Two practical water management schemes with low anode channel gas velocities, and high reactant utilization are presented in the next section. In order to capture the distributed nature of the system, a model of the water transport through the membrane and GDLs to the cathode and anode channels is needed. This channel to channel modeling domain is denoted as Through Membrane Model (TMM). One such TMM based on our previous work [8], is summarized here briefly. Finally neutron imaging data is used to (a) identify a critical TMM parameter, the immobile saturation limit, (b) propose a simple two-phase channel flow based on gravity-driven liquid flow in the channels and (c) derive simple GDL/channel boundary conditions for the liquid water distribution inside the GDL.

TWO ANODE WATER MANAGEMENT SCHEMES

Using cell voltage and input/output measurements such as temperature and pressure we aim to develop a model which can be used to avoid both anode drying and flooding conditions, since both conditions lead to recoverable voltage losses. With this PEMFC model, the estimation of liquid flow into the channel is used both for prediction of voltage degradation, and as an indication of the level of flooding in the fuel cell.

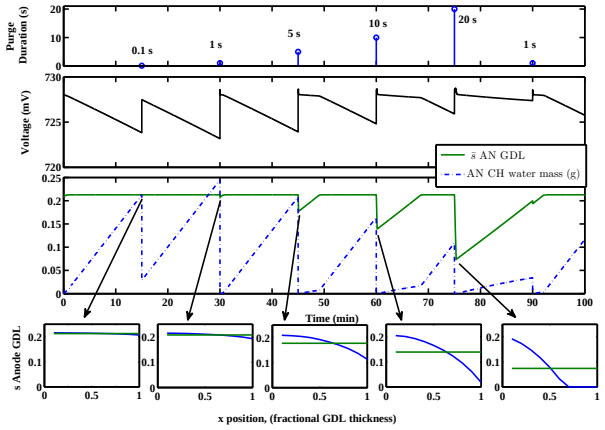

Figure 2. Effect of anode purge duration on Channel water accumulation and voltage degradation for the lumped volume TMM, for increasing purge durations of 0.1, 1, 5, 10 and 20 seconds

Two modes of operation with a dry hydrogen feed on the anode are considered in this work, and both can be modeled by extension of the TMM model. The first mode of operation is with a pressure regulated and dead-ended anode, which has 100% hydrogen utilization between purges. In this case we need to determine optimal purge period and duration. Adjusting the purge period can prevent un-necessarily large drop in voltage due to the displacement of fuel (hydrogen) in the anode channels by nitrogen [9] and liquid water [5]. For illustration of this water management scheme a simulation of the TMM is employed and shown in Fig. 2. The voltage drop predicted by the model in Fig. 2 is caused by water accumulation in the channel and the resulting reduction of catalyst area to which hydrogen is available. The high channel flow rates during the purge duration remove water from the anode channel and can also remove water from the GDL. Adjusting the purge duration can prevent unnecessary drying, as shown in the simulated experiment Fig. 2 where the

liquid water distributions inside the GDL following each purge are displayed in the last row of subplots.

The second mode of operation, uses flow-through with high utilization on the anode. In this case we determine the optimal utilization to avoid flooding near the outlet of the cell and over-drying of the inlet. Nitrogen accumulation is not a critical concern for flow though systems, but liquid water accumulation may still be an issue with low gas flow rates. Low fuel flow rate with a dry hydrogen feed is desirable, since it relieves the requirement for hydrogen grade inlet humidification systems and recirculation loops, while retaining high fuel efficiency.

Moreover, both high utilization flow-through without recirculation and dead-ended operating conditions involve low gas velocities in the channels. Due to the low gas velocity in the channel, the main mechanism for droplet detachment from the surface of the GDL is assumed to be the gravity as suggested in [4, 10] and verified by the neutron imaging data. Low gas velocity leads to the formation of large water droplets, and slugs of water may plug individual anode channels, creating portions of the cell which are effectively dead-ended until the water is removed. If a model of the liquid water and water vapor distributions can be utilized to control anode channel liquid water accumulation under these conditions, then we could potentially avoid excessive H_2 starvation that leads to carbon corrosion [6, 7]. This model can also facilitate development of control schemes that use fuel cell voltage feedback, a cheap and readily available measurement, which is closely tied to performance, to identify and avoid flooding and drying conditions.

GDL & CHANNEL WATER FRONT EVOLUTION

The Through Membrane Model (TMM) describes the distribution of water and reactant species in the GDL using Partial Differential Equations (PDEs), along the x-direction as shown in Fig. 3. The model was originally developed in [8], and is reviewed here briefly. Liquid water transport in the GDL is governed by the volume fraction of liquid water in the GDL,

$$s(x,t) = \frac{V_l}{V_p}, \tag{1}$$

where V_l is the liquid water volume, and V_p is the open pore volume of the GDL. If there is a sufficient volume of water in the porous medium, termed the immobile saturation limit s_{im}, such that there exists connected liquid pathways then liquid water can flow easily. When s falls below a this critical value, there is no liquid flow though the GDL. The reduced water saturation $S(x,t)$, captures this phenomena, where $S(x,t) = \frac{s(x,t)-s_{im}}{1-s_{im}}$, and $S = 0$ for $s < s_{im}$. Liquid flow in the GDL,

$$W_l = -\varepsilon A_{fc} \rho_l \frac{K}{\mu_l} S^3 \frac{\partial P_c}{\partial S} \frac{\partial S}{\partial x}, \tag{2}$$

is driven by the gradient in capillary pressure P_c,

$$P_c = \frac{\sigma \cos(\theta_c)\sqrt{\varepsilon}}{\sqrt{K}}(1.417 - 2.12S^2 + 1.263S^3), \tag{3}$$

The PDE describing liquid distribution water in the GDL is given by,

$$\frac{\partial s}{\partial t} = -\frac{1}{\varepsilon A_{fc} \rho_l} \frac{\partial W_l}{\partial x} - \frac{M_v}{\rho_l} r_v(c_{v,an}), \tag{4}$$

where M_v is the vapor molar mass, and ρ_l is the density of the liquid water. A graphical representation of the along the channel, and through membrane dimensions are shown in Fig. 3. The spatial coordinate x is used to indicate position along the GDL, with $x = 0$ at the membrane, and $x = L_{GDL}$ as the GDL-channel interface. The spatial coordinate z is used to indicate position along the channel, with $z = 0$ at the inlet, and $z = L_{ch}$ as the outlet location. The liquid water profile forms a steep front inside the GDL. Other capillary pressure models [11], [12], [13], should also exhibit a similar behavior in the formation of a steep liquid water front and propagation mode [14].

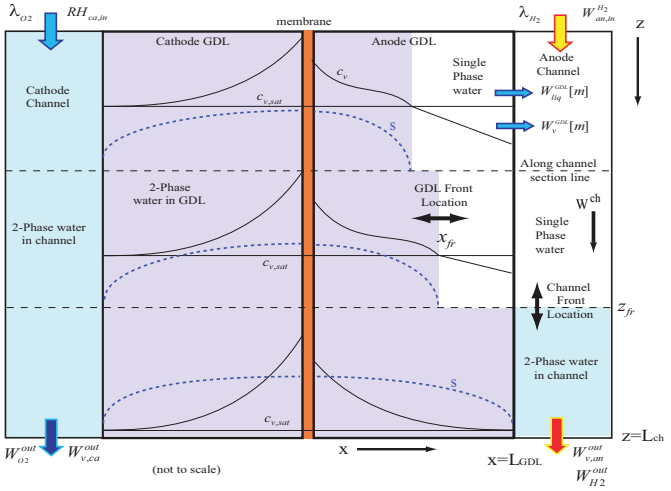

Figure 3. Schematic of along the channel model, with two-phase front for channel, and within the GDL for each unit model discretization along the channel. The x-dimension is exploded to show the distribution in water through the GDL; the physical dimensions are $L_{GDL} = 0.336$ mm and $L_{ch} = 72$ mm.

The concentration of water vapor in the GDL, $c_{v,an}$, is governed by the following PDE.

$$\frac{\partial c_{v,an}}{\partial t} = \frac{\partial}{\partial x}\left(D_v^{s_{im}} \frac{\partial c_{v,an}}{\partial x}\right) + r_v(c_{v,an}), \tag{5}$$

where $D_v^{s_{im}}$ is the diffusivity of vapor inside the GDL porous medium. The two PDEs (4)-(5) are coupled through the evaporation/condensation term $r_v(c_{v,an})$,

$$r_v(c_{v,an}) = \begin{cases} \gamma(c_v^{sat} - c_{v,an}) & \text{for } s > 0, \\ \min\{0, \gamma(c_v^{sat} - c_{v,an})\} & \text{for } s = 0 \end{cases}$$

where γ is the volumetric condensation coefficient and c_v^{sat} is the vapor saturation concentration.

The Boundary Conditions (BCs) complete the model of GDL water. For $c_{v,an}(x,t)$, mixed Neumann-Dirichlet type BC are imposed. The channel (*ch*) boundary condition is,

$$c_{v,an}|_{x=L_{GDL}} = c_{v,an}^{ch} = p_{v,an}^{ch} / (\mathcal{R}T), \tag{6}$$

where $\mathcal{R}$ is the universal gas constant, T is the temperature and $p_{v,an}^{ch}$ is the vapor partial pressure in the channel. The slope of the water vapor distribution at the membrane is determined by the water vapor flux across the membrane,

$$\left.\frac{\partial c_{v,an}}{\partial x}\right|_{x=0} = \frac{-N^{mb}}{D_v^{s_{im}}}, \tag{7}$$

where the membrane water molar flux N^{mb} is governed by electro-osmotic drag and back diffusion [8].

For the liquid water PDE, mixed BC are again imposed. Specifically, water passing into the GDL from the membrane is assumed to be in vapor form due to the presence of a microporous layer, therefore $\left.\frac{\partial S}{\partial x}\right|_{x=0} = 0$. The liquid water flux from the GDL into the channel depends on the boundary condition at the GDL-channel interface. From observation of the liquid water distribution, captured using the neutron imaging, we propose a boundary condition which is a function of the water mass in the channel,

$$S(L,t) = g(m_l^{ch}(t)), \tag{8}$$

where $m_l^{ch}(t)$ is the mass of liquid water in the channel, and $g(\cdot)$ is in general an unknown function. Other possible models include using the liquid pressure in the channel [15], or a fixed boundary condition equal to the immobile limit [14]. Observation (c), in the following section, points to a simple functional form for the unknown boundary conditions along the channel.

Liquid water accumulation in the fuel cell can be modeled by a moving front approach as shown in Fig. 4, similar to [14]. The steep drop in *s* in the GDL, shown in Fig. 3, at the transition between the two-phase and single phase water areas is the result of the sigmoidal function of the capillary pressure and requires very fine discretization of the PDEs, (4)-(5), near the two phase

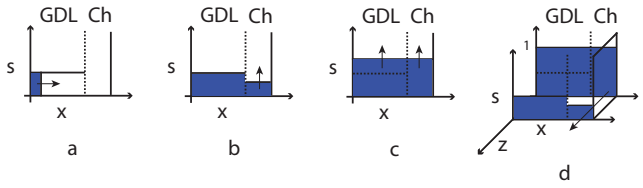

Figure 4. Evolution of liquid water fronts in the GDL and channel. In frame (a) liquid water fills the GDL up to $s = s_{im}$, then the two phase front propagates toward the channel. Next in (b) the liquid begins to accumulate in the channel. As the liquid in the channel build further, (c), there is increased resistance to liquid entering the channel and both the GDL and channel liquid volume fractions grow. Finally in (d) once the channel section fills completely water begins to spread back up along the channel.

transition in order to accurately represent the water front propagation. The caricature in Fig. 4 with a square-shape two-phase front highlights the steep transition and simplifies the PDE system to a single ordinary differential that describes the velocity of the front propagation dx/dt. This modeling paradigm will be developed further in [16].

We hypothesize that locally, Liquid water first begins to accumulate in the GDL until the volume fraction of liquid *s* reaches the immobile saturation limit s_{im}. In mode (a), the two phase liquid water front propagates toward the channel (along the x-direction) occupying a constant volume fraction, in the two phase region, which is equal the immobile limit. In the next mode, (b), the liquid water front reaches to the GDL/channel boundary. Since there is little resistance to water entering the channel, it begins to spill out of the GDL and into the channel accumulating there. As liquid water accumulates in the channel the resistance to pushing water out of the GDL increases, and the dual propagation of mode begins. In mode (c) GDL liquid water saturation is driven by the volume fraction of liquid water in the channel. Finally in mode (d), liquid water fills the anode channel section completely and begins spreading along the z-direction, up the channel and against gravity.

DATA AND OBSERVATIONS

Neutron imaging data collected at the National Institute for Standards and Technology (NIST) using a 53 cm^2 Proton Exchange Membrane Fuel Cell (PEMFC) with dead-ended anode is published in [5]. The anode gas channels are straight type flow field design, as shown in Fig. 5, with a channel width of 2.08 mm, depth of 1.78 mm, and land width of 0.838 mm. A 9-pass semi-serpentine flow path is used on the cathode, with 5 parallel paths each having a channel width of 0.686 mm, a channel depth of 0.991 mm and a land width of 0.762 mm.

Pixel intensity in the neutron images can be related to liquid water thickness t_{wl}. This measurement of water thickness is the integral of liquid water distribution along the path of the neu-

tron beam through the fuel cell. The experiments were conducted with the beam perpendicular to the membrane surface, along the x-axis, and hence provide a measurement of the liquid water distribution in only the y-z plane, as shown in Fig. 1. In order to make inferences about the water distribution in the x-direction, the fuel cell active area was divided on a 9x9 grid, shown in Fig. 5. Using the method described in [5], the local average water thickness for each of the 81 sections was estimated for each of the three layers, the Anode Channel (AN_CH), Cathode Channel (CA_CH) and the GDL Membrane sandwich (MEMB+GDL), which includes both the anode and cathode GDLs. The local water thickness in the membrane GDL sandwich layer $t_{w,MEMB+GDL}$ can be measured directly from the neutron image data by looking areas which have lands on both side of the GDL. The local Anode channel water thickness can be calculated from the difference in water thickness between $t_{w,MEMB+GDL}$ and adjacent regions with an anode channel / cathode land configuration.

Several observations from this data are presented in the following section along with connections to the relevant system dynamics. In particular we utilize the neutron imaging data of the liquid water distribution to (a) identify the immobile saturation limit, (b) propose gravity-driven liquid flow in the channels, and (c) derive new boundary conditions for the GDL channel interface.

a) Identifying the immobile limit

Although it is not possible to separate Anode GDL from Cathode GDL liquid water content due to the nature of the neutron measurements, the TMM model structure can be used to make inferences beyond direct measurement. If similar, saturated vapor, conditions exist locally in both the anode and cathode channels, and the current density is relatively low, then it is reasonable to assume that the liquid water is evenly distributed between the Anode and Cathode GDLs. Under these conditions we also assume that the water distribution between the land and channel areas is uniform. Therefore, if we consider sections of the fuel cell which exhibit mode (b) behavior, as explained in Fig. 4, then the GDL water content should be equal to the immobile saturation limit in these sections. The water thickness $t_{w,MEMB+GDL}$ from sections in flooding mode (b) can be used to find the average volume fraction of water in both GDLs $\bar{s}$ and hence the immobile saturation value using the following equation

$$\bar{s} = \frac{1}{L_{GDL}} \int_{-L_{GDL}}^{0} s_{ca}(x)\mathrm{d}x + \frac{1}{L_{GDL}} \int_{0}^{L_{GDL}} s_{an}(x)\mathrm{d}x \qquad (9)$$

$$= \frac{\bar{V}_l}{V_p} = \frac{(t_{w,MEMB+GDL} - t_{w,mb})}{2\, L_{GDL}\, \varepsilon}, \qquad (10)$$

where $t_{w,mb}$ is the water thickness in the membrane. The water thickness measurement from the neutron image, which is shown in Fig. 7(a)-7(b) indicates that the transition from GDL filling, mode (a), to channel filling, mode (b), occurs when $t_{w,MEMB+GDL} = 0.2$ mm. The membrane thickness is only 25 μm thick, hence if the membrane were completely filled with water, $t_{w,mb} < 25$ μm, which is close to the minimum resolution of the neutron imaging setup [5]. Therefore we may assume $t_{w,mb} = 25$ μm with little additional uncertainty in our estimate of $\bar{s}$. The uncompressed GDL thickness is $L_{GDL} = 0.42$ mm, and the open porosity of the GDL is $\varepsilon = 0.84$. If we assume 20 % linear compression of the GDL in the assembled cell [17], then the open porosity of the GDL drops to $\varepsilon = 0.80$, and the thickness decreases to $L_{GDL} = 0.336$ mm. Therefore the average value of saturation is $\bar{s} = 0.37 \approx s_{im}$ (assuming a 20% linear GDL compression), and is approximately equal to the immobile limit.

b) Gravity driven liquid water channel flow

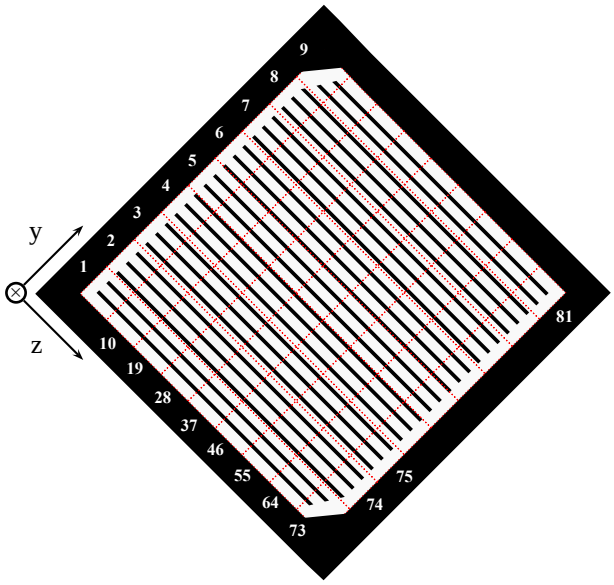

Figure 5. Anode Channel Mask

In the case of very high H_2 utilization with dry hydrogen feed and low anodic flow, the data shows that channel flooding follows the gravity-preferred direction. This implies that gravity driven flow dominates the gas flow interaction with liquid water in the channel. Once liquid water droplets reach a critical size, they may be detached from the surface of the GDL by the force of gravity [4], and flow to the bottom of the cell where the water accumulates. Three anode channels drain into each of the sections along the bottom of the fuel cell (sections 73-81), and these sections are connected in the y-direction, as seen in Fig. 5, allowing water to drain into section 73 from any other section, effectively the entire active area. In the neutron images the spreading of a liquid water film in the anode channel is observed. Due to

gravity, water collects near the outlet of the cell, section 73. The water film spreads from the bottom of the cell along the channels as shown in Fig. 7(b) from section 73 → 64 → 55 reaching up toward the inlet. The rate of water filling in each sections agrees with the hypothesized spreading film model assuming a completely filled channel. When the average water thickness in the channel for section 73 begins to level off at t=3954 (min), water begins to accumulate in the section above, 64, and again at t=3959 (min), the film spreads to section 55. These observations allow us to model the two phase channel flow as a simple moving front, where the front location z_{fr} is given by

$$\frac{dz_{fr}}{dt} = \frac{1}{\rho_l h_{ch} w_{ch}} W_l^{GDL}, \tag{11}$$

where L_{ch}, w_{ch}, and h_{ch} are the channel dimensions, and $W_l^{GDL}(z)$ is the liquid water flow from the GDL to channel calculated using the TMM by evaluating (2) at the boundary.

The ability of the TMM structure to capture the dynamic phenomena has been validated with observations from neutron imaging measurements [18]. A simulation of DEA operation with a 10 section discretization of the TMM GDL model is presented in Fig. 2. The simulation shows the impact of varying anode purge durations when a pressure regulated dry hydrogen feed is used. Longer purge durations impose drier anode channel boundary condition, and demonstrate the expected variation in liquid water distribution within the GDL resulting from the variation in channel vapor boundary conditions. The last row of subplots show snapshots in time of the liquid water distribution throughout the GDL, shown in solid blue, and the averaged value $\bar{s}$ in green. Notice that the averaged value $\bar{s}$, is all that can be inferred from the neutron imaging data. Although the agreement between measured and model predicted channel liquid water accumulation is quite good [18], if we compare the averaged liquid water saturation in the GDL $\bar{s}$ to the measured value of liquid water thickness shown in Fig. 6, we find that without consideration of the effect of channel liquid water on GDL accumulation, the model is unable to accurately capture the increased GDL water content that was observed when the channel was flooded.

c)Boundary conditions for the GDL channel interface

From the data we observe that there is no channel flooding in sections for which $t_{wl}^{GDL} < 0.2$ mm as shown in Fig. 7(a)-7(b), which corresponds to GDL accumulation mode (a). From the neutron imaging data we find that the measured GDL liquid water thickness is in the range $t_{w,MGDL}$=[0.2,0.5] mm, under the lands, when more anode channel flooding is observed, corresponding to channel flooding mode (c). Using (10), this gives a value for the average liquid saturation inside the GDL to range between $\bar{s}$=[0.37,0.93] when the anode channel is filled with water. Fig. 7(b) shows that GDL liquid water mass and channel water mass grow together when the anode channel is flooding. We

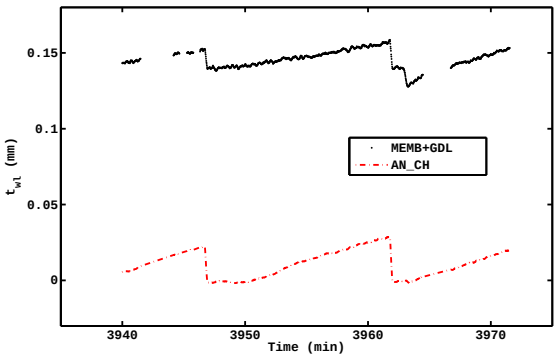

Figure 6. Cell averaged liquid water thickness for the same experimental conditions shown in Fig. 7

hypothesize that the channel drives the GDL through boundary condition (8), and that

$$g(m_l^{ch}(t)) = \frac{m_l^{ch}(t)}{\rho_l \, h_{ch} \, w_{ch} \, L_{ch}} \tag{12}$$

MODEL EXTENSION TO 1+1D

The benefit of reduced model complexity becomes apparent, as the use of computationally inexpensive analytic solutions frees up cpu time allowing for increased resolution in the GDL x-coordinate direction and/or discretization along the channel. The spatial coordinate z, shown in Fig. 3, is used to indicate position along the channel, with $z = 0$ at the inlet, and $z = L_{ch}$ as the outlet location.

Under the assumptions of uniform current density, temperature and saturated cathode conditions, the anode GDL conditions are described by the TMM model with constant boundary conditions for the cathode channel, and spatially varying boundary conditions for the anode channel. The spatially varying boundary conditions include channel concentrations of hydrogen, $c_{H_2}^{ch}(z)$, water vapor, $c_{v,an}^{ch}(z)$, and the mass of liquid water in the channel , $m_{l,an}^{ch}(z)$. Fig. 3 illustrates the uniform cathode conditions and the two phase front location, x_{fr}, in the anode GDL where s reaches zero. There also exists a single phase to two phase water transition region along the length of the anode channel, denoted as z_{fr}. Due to the long aspect ratio of the channel relative to the GDL thickness, we can implement a 1+1D modeling approach where the coupling in the z direction is only through the channel states, and hence the boundary conditions of each TMM unit cell model.

CONCLUSIONS

We review a control oriented through the membrane model and show the spatial variation in water along the channel by cou-

pling the TMM model with an along the channel extension. We formulate the purge and flow-through control modes and potential control objectives. We use neutron imaging to extract important model parameters such as the immobile saturation limit s_{im} and the channel boundary conditions for s. The data is also used to propose a model simplification in terms of liquid water accumulation in the anode channel driven by gravity when the gas velocity is sufficiently small.

ACKNOWLEDGMENT

This work was supported by the National Science Foundation (CMS 0625610), the U.S. Department of Energy (DE-FG02-06CH 11300), the U.S. Department of Commerce, the NIST Ionizing Radiation Division, the Director's Office of NIST, the NIST Center for Neutron Research, and the Department of Energy through interagency agreement no. DE-AI01-01EE50660.

REFERENCES

[1] Chen, K. S., Hickner, M. A., and Noble, D. R., 2005. "Simplified models for predicting the onset of liquid water droplet instability at the gas diffusion layer/gas flow channel interface". *International Journal of Energy Research*, **29**(12), pp. 1113–1132.

[2] Kumbur, E., Sharp, K., and Mench, M., 2006. "Liquid droplet behavior and instability in a polymer electrolyte fuel cell flow channel". *Journal of Power Sources*, **161**(1), Oct., pp. 333–345.

[3] Zhang, F. Y., Yang, X. G., and Wang, C. Y., 2006. "Liquid water removal from a polymer electrolyte fuel cell". *Journal of The Electrochemical Society*, **153**(2), pp. A225–A232.

[4] Schillberg, Charles H. Kandlikar, S. G., 2007. "A review of models for water droplet detachment from the gas diffusion layer-gas flow channel interface in PEMFC's". In Proceedings of the 5th International Conference on Nanochannels, Microchannels and Minichannels, ICNMM200, Vol. B, pp. 299–310.

[5] Siegel, J. B., McKay, D. A., Stefanopoulou, A. G., Hussey, D. S., and Jacobson, D. L., 2008. "Measurement of liquid water accumulation in a PEMFC with dead-ended anode". *Journal of The Electrochemical Society*, **155**, pp. B1168–B1178.

[6] Meyers, J. P., and Darling, R. M., 2006. "Model of Carbon Corrosion in PEM Fuel Cells". *J. Electrochem. Soc.*, **153**(8), Aug., pp. A1432–A1442.

[7] Franco, A. A., and Gerard, M., 2008. "Multiscale model of carbon corrosion in a pefc: Coupling with electrocatalysis and impact on performance degradation". *J. Electrochem. Soc.*, **155**(4), Apr., pp. B367–B384.

[8] McKay, D. A., Siegel, J. B., Ott, W., and Stefanopoulou, A. G., 2008. "Parameterization and prediction of temporal fuel cell voltage behavior during flooding and drying conditions". *Journal of Power Sources*, **178**(1), Mar., pp. 207–222.

[9] Kocha, S. S., Yang, J. D., and Yi, J. S., 2006. "Characterization of gas crossover and its implications in PEM fuel cells". *AIChE Journal*, **52**(5), pp. 1916–1925.

[10] Kimball, E., Whitaker, T., Kevrekidis, Y. G., and Benziger, J. B., 2008. "Drops, slugs, and flooding in polymer electrolyte membrane fuel cells". *AIChE Journal*, **54**(5), pp. 1313–1332.

[11] Gostick, J. T., Fowler, M. W., Ioannidis, M. A., Pritzker, M. D., Volfkovich, Y., and Sakars, A., 2006. "Capillary pressure and hydrophilic porosity in gas diffusion layers for polymer electrolyte fuel cells". *Journal of Power Sources*, **156**(2), June, pp. 375–387.

[12] Markicevic, B., Bazylak, A., and Djilali, N., 2007. "Determination of transport parameters for multiphase flow in porous gas diffusion electrodes using a capillary network model". *Journal of Power Sources*, **171**(2), pp. 706 – 717.

[13] Kumbur, E. C., Sharp, K. V., and Mench, M. M., 2007. "Validated leverett approach for multiphase flow in pefc diffusion media ii. compression effect". *Journal of The Electrochemical Society*, **154**(12), pp. B1305–B1314.

[14] Promislow, K., Chang, P., Haas, H., and Wetton, B., 2008. "Two-phase unit cell model for slow transients in polymer electrolyte membrane fuel cells". *Journal of The Electrochemical Society*, **155**(7), pp. A494–A504.

[15] Grtsch, M., and Mangold, M., 2008. "A two-phase pemfc model for process control purposes". *Chemical Engineering Science*, **63**(2), pp. 434 – 447.

[16] Siegel, J. B., and Stefanopoulou, A. G., 2009. "Through the Membrane & Along the Channel Flooding in PEMFCs". In Proceedings of the 2009 American Control Conference. Paper ThA20.4.

[17] Gostick, J. T., Fowler, M. W., Pritzker, M. D., Ioannidis, M. A., and Behra, L. M., 2006. "In-plane and through-plane gas permeability of carbon fiber electrode backing layers". *Journal of Power Sources*, **162**(1), Nov., pp. 228–238.

[18] Siegel, J., McKay, D., and Stefanopoulou, A., 2008. "Modeling and validation of fuel cell water dynamics using neutron imaging". In Proceedings of the 2008 American Control Conference, pp. 2573–2578.

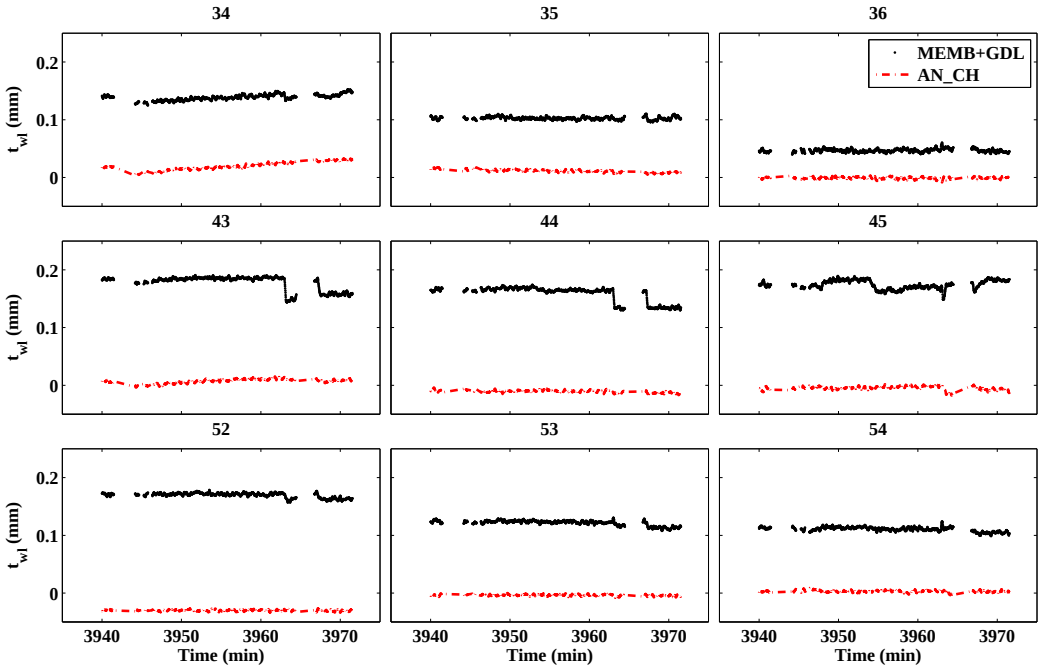

(a) Liquid water thickness at the middle of the cell

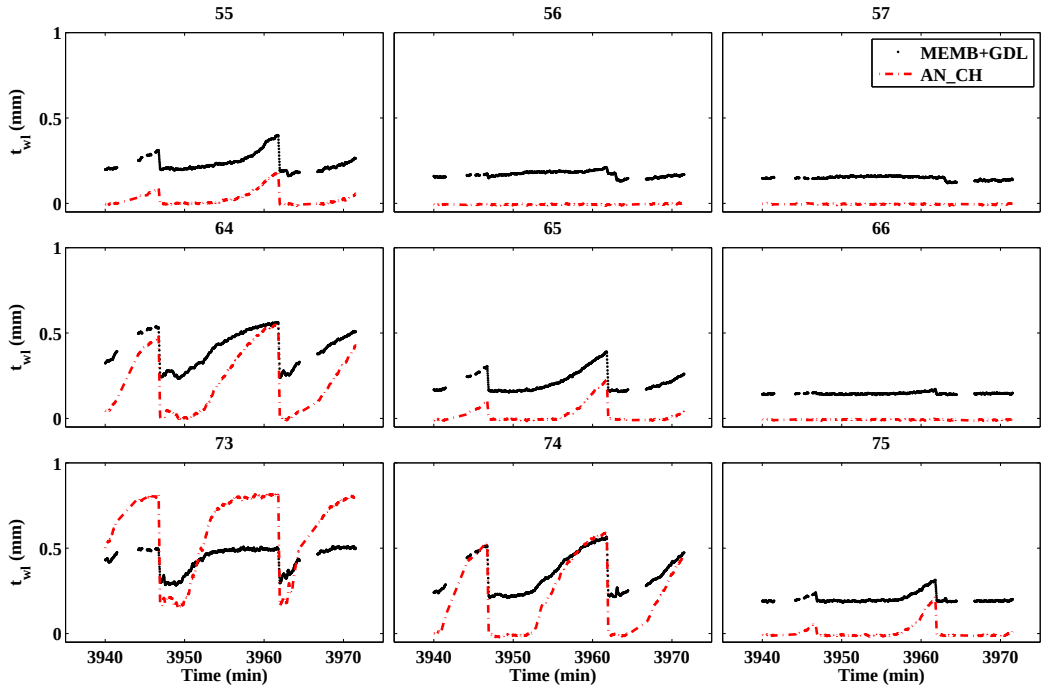

(b) Liquid water thickness at the end of the anode channels

Figure 7. Average liquid water thickness over each section, as estimated from the by neutron imaging; showing water accumulation in the AN_GDL+Membrane+CA_GDL and anode channel, along the height of adjacent anode channels. These experiments were conducted with fully humidified air at a current density of 378 mA cm^{-2}, a cell operating temperature of 50°C, and an air stoichiometry of 300%